Journal of Magnetism and Magnetic Materials 560 (2022) 169523

Contents lists available at ScienceDirect

Journal of Magnetism and Magnetic Materials

journal homepage: www.elsevier.com/locate/jmmm

Microwave absorption performance of M-type hexagonal ferrite and MXene composite in K_a and V bands (5G mmWave frequency bands)

Hoyun Won [a], Yang-Ki Hong [a,*], Minyeong Choi [a], Hector Garcia [b], Dongmyung Shin [c], Young-Sik Yoon [c], Kwangjoo Lee [c], Hao Xin [b], Chang-Dong Yeo [d]

[a] Department of Electrical and Computer Engineering, The University of Alabama, Tuscaloosa, AL 35487, USA
[b] Department of Electrical and Computer Engineering, The University of Arizona, Tucson, AZ 85719, USA
[c] Semiconductor Materials R&D/Advanced Materials, LG CHEM, LG Science Park, Magokjungang, Gangseo-gu, Seoul 07796, Republic of Korea
[d] Department of Mechanical Engineering, Texas Tech University, Lubbock, TX 79409, USA

ARTICLE INFO

Keywords:
Absorber
Electromagnetic interference
Ferromagnetic resonance
Hexaferrite
MXene
Shielding effectiveness

ABSTRACT

Lightweight and thin electromagnetic interference (EMI) shielding materials with high shielding effectiveness (SE) have been investigated over the last decade to address the unreliability issue in all electronic technologies caused by EMI. Herein, we report the SE of the novel $Ti_3C_2T_x$ MXene/doped-hexaferrite (hexagonal ferrite: $BaCo_{0.3}Ti_{0.3}Fe_{11.4}O_{19}$) composite. This composite suppresses electromagnetic (EM) waves dominantly via absorption over the frequency range from 30 to 50 GHz for millimeter-wave (mmWave) applications. Two-dimensional inorganic compound $Ti_3C_2T_x$ MXene was synthesized using the LiF-HCl etching process, and doped-hexaferrite particles were prepared using a conventional solid-state reaction. Then, the MXene/doped-hexaferrite composite was fabricated by mixing MXene/polyvinyl-pyrrolidone (PVP) containing solution with the hexaferrite particles. The composites were characterized by a vibrating sample magnetometer for static magnetic properties and a vector network analyzer for dynamic magnetic and dielectric properties and microwave absorbing performance.

A high magnetocrystalline anisotropy of hexaferrite shifted the microwave absorption peak to mmWave bands such as K_a- and V-bands, unlike spinel ferrite. The 1.5 mm thick MXene/45 wt% doped-hexaferrite composite shows a broad effective bandwidth (reflection loss (RL) less than 10 dB) of 7 GHz in the frequency range from 38 to 45 GHz. This excellent absorbing performance is mainly attributed to improved impedance matching and enhanced dielectric and magnetic losses of the composite. It was found that the SE was dominated by absorption instead of reflection.

The experimental results demonstrate that the MXene/$BaCo_{0.3}Ti_{0.3}Fe_{11.4}O_{19}$ hexaferrite composite can be a promising and effective EM wave absorber material for millimeter-wave applications such as the fifth-generation (5G) network and opens up new opportunities for THz (6G network) EMI materials development.

1. Introduction

The growing scales and devices in the modern microwave spectrum (3–30 GHz) necessitate the cellular and telecommunication industries to look for other high-frequency ranges to support upcoming devices requiring large bandwidth and high data rates. Accordingly, electronic device operation frequency moves from Sub-6 GHz 5G (fifth generation) spectrum to the high GHz band (mmWave 5G). The millimeter-wave (mmWave) spectrum covers 30–300 GHz, and the radiation in the mmWave band causes more electromagnetic interference (EMI) than the lower frequency spectrum. The EMI causes data loss, data misinterpretation, and malfunction of electronic components near EMI sources due to cross-talk between devices or components in electronic systems. Therefore, lightweight and thin EMI shielding materials with high shielding effectiveness (SE) have been investigated over the last decade. Three interaction phenomena characterize shielding characteristics of EMI material [1]: Reflection of incident microwave; absorption; multiple reflections inside layered materials. Thus, the shielding materials must minimize reflected microwaves from the interface between the air and the material, enhancing microwave absorption and attenuating

* Corresponding author.
E-mail address: ykhong@eng.ua.edu (Y.-K. Hong).

https://doi.org/10.1016/j.jmmm.2022.169523
Received 2 February 2022; Received in revised form 18 May 2022; Accepted 23 May 2022
Available online 11 June 2022

transmitted microwaves. The total SE (SE_T) of EM absorbing material is a sum of reflection SE (SE_R), absorption SE (SE_A), and multiple reflection SE (SE_M). In general, the EM shielding by the multiple reflections is weaker than the other two, therefore making a negligible contribution to the total shielding.

To attenuate EMI, microwave absorbing materials (MAM) in the S band (2–4 GHz), C (4–8 GHz), X (8–12 GHz), and Ku (12–18 GHz) bands are in great demand [2–5]. Highly electrically conductive SE materials have been quested during the last decade. Composition $Ti_3C_2T_x$ (T_x = surface moiety, *i.e.*, a mixture of —OH, =O, and —F), namely MXene, possesses the highest electrical conductivity among MXenes [6] and is a nano-layered structure such as flakes [7]. Thus, the MXene reflects the incident microwave at its surface and the interfaces between nanoflakes (laminated structure). High electrically conductive SE material weakly interacts with a microwave but reflects the incident microwave, while a low conductive SE material does pass the microwave, therefore, absorbing the wave [8].

Recently, it was reported that 45 μm thick $Ti_3C_2T_x$ MXene exhibits a high SE_T of 92 dB in 8–12 GHz (X band) [9]. This high SE_T is attributed to the high intrinsic conductivity of 4600 Siemens/cm. About 60% of the SE_T comes from microwave absorption and 40% from the reflection. On the other hand, the 1.68 μm thick $Ti_3C_2T_x$ MXene shows that the SE_T is dominated by a reflection contribution of about 98% [10]. This result is opposite to the SE_T result in [9]. This disagreement is not discussed in this paper. However, the reflection is undesirable because the reflected microwave affects neighboring components in the electronic systems or provides unreliability in electronic technologies. Therefore, an impedance matching of MXene is still an issue to be addressed to enhance magnetic and dielectric losses' contribution to SE_T, thus, depressing the reflection.

To improve the impedance matching of $Ti_3C_2T_x$ MXene, magnetic particles are embedded in MXene flakes. The magnetic particle is a metallic element, spinel ferrite, or hexaferrite (hexagonal ferrite). The 1.75 mm thick MXene/Ni composite shows the minimum reflection loss (RL_{min}) of 49.9 dB at 11.9 GHz [11]. When ferromagnetic Co replaces Ni, the 1.02 nm thick MXene/Co nanochain shows an RL_{min} of 46.48 dB at 16.75 GHz [12]. It is noted that Co shifted the RL_{min} frequency to 16.75 GHz from 11.9 GHz. This is because the magneto-crystalline anisotropy field (H_a) of Co is higher than that of Ni, *i.e.*, higher ferromagnetic resonant frequency (f_{FMR}). Electrically conductive and ferromagnetic Fe-Co alloy particles were embedded in MXene to obtain high-magnetic loss due to its high saturation magnetization [3]. As a result, the effective absorption band (EAB) of MXene/FeCo composite increased to 8.8 GHz (9.2–18.0 GHz) from 6.3 GHz of MXene/Ni composite. Deng *et al.* reported the RL_{min} of 45.5 dB and the EAB of 3.5 GHz (8–10.5 GHz) in the X-band for a 1.6 mm thick $Ti_3C_2T_x/Fe_3O_4$@C hybrid [13]. When spinel ferrite ($Ni_{0.5}Zn_{0.5}Fe_2O_4$) was incorporated in MXene, the RL peak (resonant frequency) shifted to 13.5 GHz from about 9 GHz of the MXene/Fe_3O_4 composite. Once again, this is attributed to the H_a of spinel ferrite than that of soft magnetite (Fe_3O_4). Accordingly, the 6.5 mm thick $Ti_3C_2T_x/Ni_{0.5}Zn_{0.5}Fe_2O_4$ composite shows an RL_{min} of 42.5 dB at 13.5 GHz and EAB of 3 GHz (12–15 GHz) in the Ku-band [14]. When $Ni_{0.5}Zn_{0.5}Fe_2O_4$ ferrite was replaced by $ZnFe_2O_4$ ferrite, the f_{FMR} shifted to a higher frequency than 13 GHz. As a result, 7.5 mm thick $Ti_3C_2T_x/ZnFe_2O_4$ composite shows an RL_{min} of 60.94 dB at 14.72 GHz and EAB of 6.08 GHz (11.92–18 GHz) [15].

To realize EMI suppression in the mmWave band by microwave absorption, magnetic materials such as hexaferrite with a high H_a are needed. Magnetic loss, *i.e.*, the imaginary part of complex permeability, rapidly increases near the f_{FMR}. The f_{FMR} is determined by H_a of a magnetic material and is adjustable by substituting Fe of M−type pure hexaferrite ($SrFe_{12}O_{19}$ or $BaFe_{12}O_{19}$) with other elements. M−type pure hexaferrite ($SrFe_{12}O_{19}$ or $BaFe_{12}O_{19}$) holds 17 kOe of H_a, corresponding to about 40–50 GHz of the $f_{FMR.}$ Hexaferrite is chemically stable and has a high Curie temperature, therefore a good component for microwave absorption material composites. Kim *et al.* doped a pure M−type $SrFe_{12}O_{19}$ with Zn and Zr to lower the H_a, adjusting the f_{FMR} to the Ku-band. $SrFe_{12-2x}$ $Zn_xZr_xO_{19}$ (x = 0.9) hexaferrite shows a high EM absorption of the RL_{min} of 45 dB and EAB of 7 GHz in the X-band (8–12 GHz) [16]. Dong *et al.* reported an RL_{min} of 45 dB and EAB of 9.5 GHz (29–38.5 GHz) of doped-hexaferrite [$BaCo_xTi_xFe_{12-2x}O_{19}$ (x = 0.5)] in the K_a-band [17]. The above results imply that high magnetocrystalline anisotropy, saturation magnetization, and electrical resistive materials are desired for MXene composite, operating in K_a- and V-bands (5G mmWave frequency bands). However, no MXene/M−type hexaferrite composite and its shielding effectiveness in K_a- and V-bands were reported.

In this paper, we studied the SE of the novel $Ti_3C_2T_x$ MXene/doped-hexaferrite ($BaCo_{0.3}Ti_{0.3}Fe_{11.4}O_{19}$) composite by measuring the frequency dependence of both complex permittivity and permeability and reflection loss (RL) in K_a- and V-bands (30–50 GHz: 5G mmWave frequency bands). The H_a of M−type pure $BaFe_{12}O_{19}$ hexaferrite is adjusted to a H_a suitable for K_a- and V-bands by doping M−type $BaFe_{12}O_{19}$ with a couple of Co and Ti elements. Doped-hexaferrite ($BaCo_{0.3}Ti_{0.3}Fe_{11.4}O_{19}$) particles are synthesized and incorporated into MXene flakes, making an MXene/hexaferrite composite.

2. Materials and methods

2.1. Preparation of $Ti_3C_2T_x$ MXene

Ti_3AlC_2 powder (purity ≥ 99.0 %) was purchased from Nanoshel-UK Ltd, UK. Hydrochloric acid (HCl, 12 M) and lithium fluoride (LiF, purity ≥ 99.99 %) were obtained from VWR International, USA. $BaCO_3$ (purity ≥ 99.0%) and Fe_2O_3 (purity ≥ 99.0%) were purchased from Sigma Aldrich, USA, while TiO_2 and Co_2O_3 were obtained from Alfa Aesar, USA, and SkySpring Nanomaterials, Inc, USA, respectively. Lastly, PVP was purchased from G-Biosciences, USA.

$Ti_3C_2T_x$ MXene were synthesized via the LiF-HCl etching process. Two grams of LiF powder were slowly poured into 40 mL 9 M HCl solution in a Teflon container. The LiF containing HCl solution was stirred with a magnetic stirrer for 30 min at room temperature. Then, 2 g of Ti_3AlC_2 MAX-phase powder was added slowly into the solution while magnetic stirring for 24 h at 35 °C. After stirring, the reaction mixture was repeatedly washed with deionized water by centrifugation at 3500 rpm until its pH reached 6 to separate multilayer MXene. The suspension was ultrasonicated for 20 min to exfoliate the MXene nanosheet and centrifuged at 3500 rpm to obtain the exfoliated nanosheets.

2.2. Preparation of Doped-Hexaferrites ($BaCo_{0.3}Ti_{0.3}Fe_{11.4}O_{19}$)

Doped-hexaferrite ($BaCo_{0.3}Ti_{0.3}Fe_{11.4}O_{19}$) powder was prepared by the conventional solid-state process [17]. The precursors, $BaCO_3$, TiO_2, Co_2O_3, and Fe_2O_3, were mixed in an appropriate stoichiometric ratio and wet milled for 2 h using a high-energy ball milling machine (Spex SamplePrep 8000D) at 1725 rpm. Then, the well-mixed powder was calcined at 1315 °C for 2 h in air. After being grounded thoroughly, the mixture was sintered at 1310 °C for 2 h in the air. The sintering heat rate was 3 °C/min.

2.3. Preparation of $Ti_3C_2T_x$ MXene/Doped-Hexaferrite ($BaCo_{0.3}Ti_{0.3}Fe_{11.4}O_{19}$) composite

The obtained MXene was dispersed into 50 mL of deionized water. Then, 2.5 g of PVP was dissolved into the solution and ultrasonicated for 20 min. After ultrasonication, $BaCo_{0.3}Ti_{0.3}Fe_{11.4}O_{19}$ hexaferrite was added to the mixture and stirred for 12 h with a nonmagnetic stirrer. Finally, the mixture was centrifuged and dried in a vacuum oven to MXene/$BaCo_{0.3}Ti_{0.3}Fe_{11.4}O_{19}$ composite. Fig. 1 illustrates the overall fabrication process.

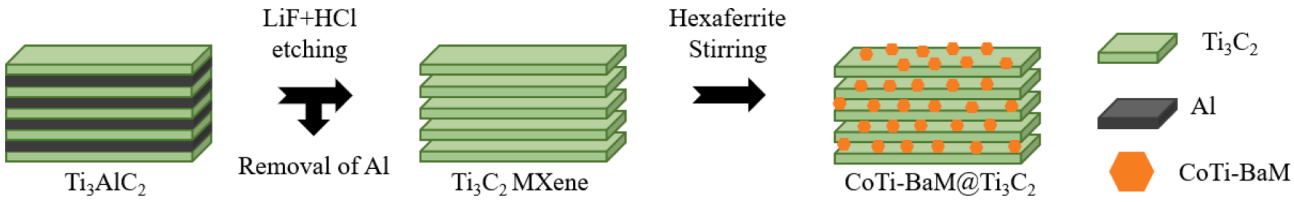

Fig. 1. Schematic illustration of MXene/doped-hexafererite ($BaCo_{0.3}Ti_{0.3}Fe_{11.4}O_{19}$: CoTi-BaM) composite synthetic process.

2.4. Characterization

An X-ray diffractor (XRD: Bruker D8 Discover) using Cu Kα radiation (λ = 0.154 nm) was used to identify the crystalline phases of MXene ($Ti_3C_2T_x$), doped-hexaferrite ($BaCo_{0.3}Ti_{0.3}Fe_{11.4}O_{19}$), and MXene/doped-hexaferrite composite. Microstructures of the developed composite were characterized with a field-emission scanning electron microscope (FE-SEM: JEOL 7000FE). A vibrating sample magnetometer (VSM: MicroSense EV9) was used to measure the static magnetic properties of the composites. The powder samples were mixed with paraffin wax at a weight ratio of 5:1 and then pressed into a rectangular shape with a length of 5.69 mm and width of 2.84 mm. A vector network analyzer (VNA: Agilent PNA-E8361A) with a WR-22 rectangular waveguide as a test fixture was used to measure complex magnetic permeability ($\mu_r = \mu' + \mu''$) and dielectric (electrical) permittivity ($\varepsilon_r = \varepsilon' + \varepsilon''$) in 30 to 50 GHz. The Nicolson-Ross-Weir approach [18] was implemented to extract μ_r and ε_r from the measured S-parameters.

3. Results AND DISCUSSION

3.1. X-ray diffraction and scanning electron microscopy

Fig. 2 shows the measured XRD patterns of the Ti_3AlC_2 MAX, $Ti_3C_2T_x$ MXene, doped-hexaferrite ($BaCo_{0.3}Ti_{0.3}Fe_{11.4}O_{19}$), and MXene/doped-hexaferrite composite. The diffraction peaks at 2θ values of 9.7, 39, 41.2, and 60.5° correspond to the (002), (104), (105), and (110) planes, respectively. These planes match the reported MAX phase (JCPDS card no. 52-0875). After the LiF/HCl mixture solution treatment, the characteristic peaks at 2θ of 39° disappeared; therefore, Al elements were removed [19]. Further, the characteristic diffraction peak (002) of MAX is shifted to 7.3° from 9.7°, implying the enlarged interlayer spacing and formation of laminated and exfoliated MXene [19]. The XRD pattern also showed that doped-hexaferrites are formed well as the diffraction peaks appear at 2θ = 22.9, 30.3, and 63.1° [17]. For the MXene/doped-hexaferrite ($BaCo_{0.3}Ti_{0.3}Fe_{11.4}O_{19}$) composite, the main diffraction peaks of the MXene and doped-hexaferrite were also confirmed, demonstrating the successful synthesis of the desired composite without any crystal structure changes.

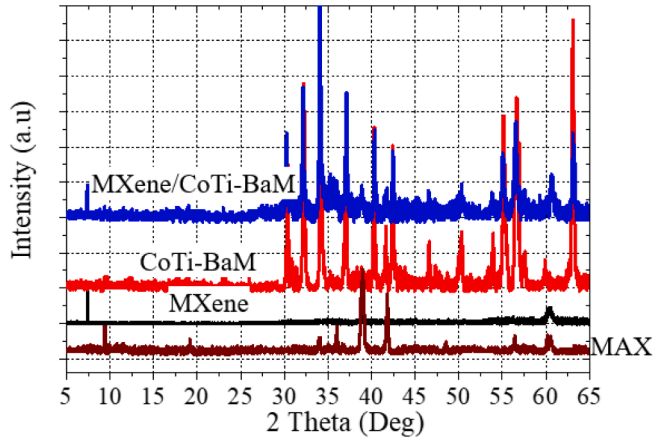

Fig. 2. XRD patterns of Ti_3AlC_2 MAX, MXene, doped-hexaferrite ($BaCo_{0.3}Ti_{0.3}Fe_{11.4}O_{19}$: CoTi-BaM), and MXene/doped-hexaferrite composite.

The microstructure and morphology of the synthesized MXene and MXene/doped-hexaferrite ($BaCo_{0.3}Ti_{0.3}Fe_{11.4}O_{19}$) composite were characterized by a scanning electron microscope (SEM). Fig. 3(a) shows an accordion-like morphology of the synthesized MXene. This result confirms the removal of the Al layer from the MAX phase [2]. It is seen that hexagonal-shaped doped-hexaferrite particles with an average particle size of 1–3 μm are embedded in and attached firmly to the surface of the laminated MXene. The XRD and SEM characterization results confirm MXene/doped-hexaferrite composite is well formed.

3.2. Static magnetic properties

Fig. 4 shows the magnetic M−H hysteresis loops of MXene, doped-hexaferrite ($BaCo_{0.3}Ti_{0.3}Fe_{11.4}O_{19}$), and MXene/doped-hexaferrite composites with different contents of doped-hexaferrite (20, 30, and 45 wt%) measured in the range of applied magnetic field from −20 kOe to + 20 kOe. The saturation magnetization (σ_s) and intrinsic coercivity (H_{ci}) of the doped-hexaferrite are 66.5 emu/g and 401 Oe, respectively, close to the reported data [17]. As the content of doped-hexaferrite increases from 0 to 45 wt%, the σ_s increases from 0 emu/g to 4.5 emu/g (20 wt%) to 9.7 emu/g (30 wt%) to 21.5 emu/g (45 wt%), and H_{ci} also increases from 0 Oe to 186 Oe (20 wt%) to 245 Oe (30 wt%) to 285 Oe (45 wt%). An increase in the σ_s and H_{ci} of the composite is mainly attributed to the reduction of paramagnetic MXene content, demonstrating MXene/doped-hexaferrite composite. As a result, it is seen that the magnetic hysteresis loop gradually becomes more significant as the content of doped-hexaferrite increases, implying that magnetic hysteresis loss increases.

3.3. Dynamic magnetic, dielectric, and absorption properties

EM wave absorption and RL were calculated by the following equations based on the transmission line theory:

$$R_L(dB) = 20\log|(Z_{in} - Z_0)/(Z_{in} + Z_0)| \quad (1)$$

$$Z_{in} = Z_0\sqrt{\mu_r/\varepsilon_r}\tanh\left[j(2\pi fd/c)\sqrt{\mu_r\varepsilon_r}\right] \quad (2)$$

where Z_{in} is the input impedance, Z_0 represents the free-space impedance of 377 Ω, f is the frequency in Hz, c is the speed of light in free space, and d is the thickness of the material. Fig. 5 shows the measured frequency-dependent relative permittivity (ε_r) and relative permeability (μ_r) of MXene/doped-hexaferrite composite. The real part of ε_r (ε') decreases as the content of doped-hexaferrite increases from 20 to 45 wt% for f below 38 GHz. For f above 38 GHz, the ε' slightly increases and then significantly decreases as shown in Fig. 5(a). As for the imaginary permittivity (ε'') in Fig. 5(b), MXene/doped-hexaferrite (20 wt%) composite shows a significantly higher ε'' of 3.0–3.5 than 0–1.5 of 30 or 45 wt% doped-hexaferrite composite in the range of 30 to 50 GHz. This decrease in ε_r with respect to an increase of the content of doped-hexaferrite is because hexaferrite is an electrical insulator. It is reported that when the content of semiconductor-like Fe_3O_4 increased in MXene/Fe_3O_4 composite, both electrical conductivity and ε_r decreased [20]. According to the free electron theory, the higher the electrical

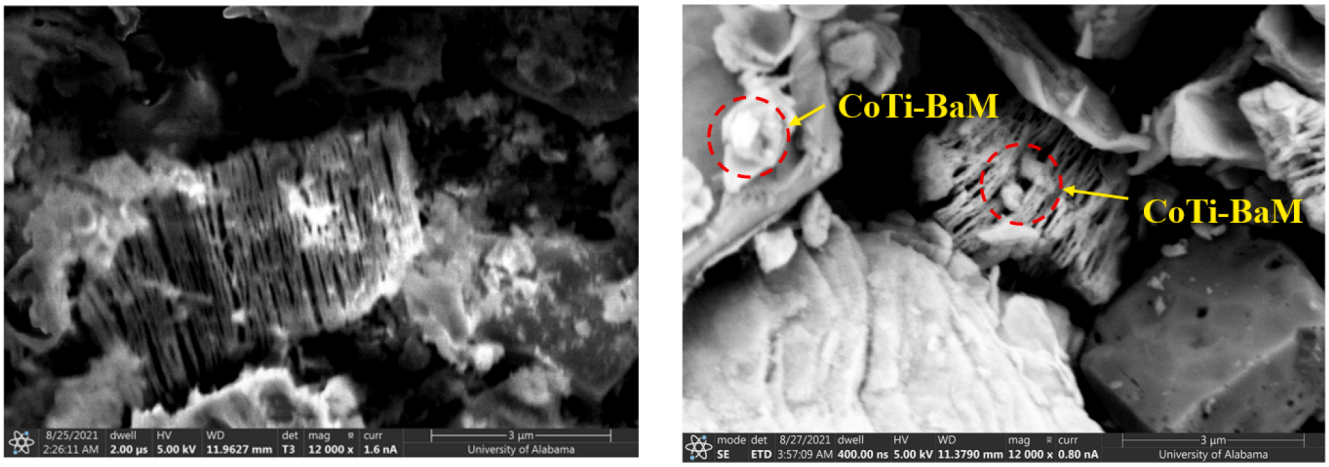

(a) (b)

Fig. 3. SEM images of (a) MXene and (b) MXene/doped-hexaferrite ($BaCo_{0.3}Ti_{0.3}Fe_{11.4}O_{19}$: CoTi-BaM) composite.

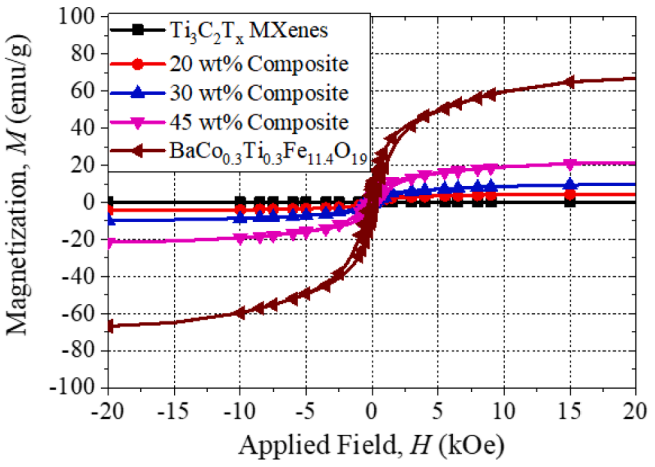

Fig. 4. Magnetic hysteresis loops of MXene, doped-hexaferrite ($BaCo_{0.3}Ti_{0.3}Fe_{11.4}O_{19}$: CoTi-BaM), and MXene/doped-hexaferrite (20, 30, and 45 wt %) composite.

conductivity, the higher the ε_r [20]. Thus, adding the insulator-like hexaferrite to highly conductive MXene lowers the conductivity of the MXene/hexaferrite composite. Therefore, the composite's ε_r decreases. This decrease in ε_r with spinel ferrite was observed in many MXenes/magnetic material composites such as MXene/$NiFe_2O_4$ [4] and MXene/$CoFe_2O_4$ [5]. Further, the ε'' signifies the dielectric energy loss in a medium. A decrease in ε'' with the content of doped-hexaferrite implies that the contribution of mitigating EMI by the dielectric energy loss is reduced. Moreover, ε' and ε'' fluctuations are attributed to the dipole polarization in MXene, which cannot catch up with the change of electric field in the frequency of interests [4].

Fig. 5(c) and (d) show that the frequency-dependent real (μ') and imaginary permeability (μ'') of MXene/doped-hexaferrite (20, 30, 45 wt %) composites are much more dispersed or fluctuated than the relative permittivity. This is attributed to multiple ferromagnetic resonances of hexaferrite, especially in MXene/45 wt% doped-hexaferrite composite. The μ' of the composite increases up to 38 GHz as the content of doped-hexaferrite increases and then decreases due to ferromagnetic resonance. The imaginary part μ'' in Fig. 5(d) shows a similar response to applied frequency to the μ'. It is noted, however, that 45 wt% doped-hexaferrite composite shows the highest magnetic loss over the frequency range of 30 to 43 GHz.

RL was measured for MXene, MXene/doped-hexaferrite (20, 30, and 45 wt%) composite, and doped-hexaferrite ($BaCo_{0.3}Ti_{0.3}Fe_{11.4}O_{19}$) to estimate how much power is reflected from EMI material. Fig. 6 shows the measured RL. There is no significant effective absorption for MXene and MXene/20–30 wt% doped-hexaferrite composites. However, the absorbing and transmission losses were significantly increased with increasing the doped-hexaferrite content. Among the measured composites, the MXene/45 wt% doped-hexaferrite composite showed the widest effective bandwidth (RL less than 10 dB) of 7 GHz (38–45 GHz). This implies the impedance matching is better than other MXene/doped-hexaferrite composites, according to Eq. (2).

The MXene/45 wt% doped-hexaferrite composites with different thicknesses were prepared and characterized for the RL over the range of 30 to 50 GHz to understand the thickness dependence of RL. Fig. 7 shows a two-dimensional plot to visualize three-dimensional data (thickness-frequency-RL). It was reported that EAB shifts to a lower frequency as the thickness increases [2]. According to the quarter wavelength theory, the matching thickness is inversely proportional to the matching frequency [21].

Lastly, the SE_T, SE_A, and SE_R of 1.5 mm thick MXene and MXene/45 wt% $BaCo_{0.3}Ti_{0.3}Fe_{11.4}O_{19}$ composite are calculated in dB according to the following equations [22]. The results are presented in Fig. 8.

$$SE_T = 10\log\left(1/|S_{21}|^2\right) \quad (3)$$

$$SE_A = 10\log\left(\left(1-|S_{11}|^2\right)/|S_{21}|^2\right) \quad (4)$$

$$SE_R = 10\log\left(1/\left(1-|S_{11}|^2\right)\right) \quad (5)$$

The calculated average SE_T of the composite was 12 dB (equivalent to 94% shielding), and the composite absorbs EM wave 83.2 % and reflects 16.8%. The composite showed 0.46–2.21 dB higher SE_T and 28.9% higher SE_A than MXene.

A comparison of this work with the reported results is made in Table 1. The novelty of this work includes the use of high magneto-crystalline anisotropy hexaferrite for composite, covering K_a and V bands (mmWave spectrum), and enhancement of magnetic loss at K_a and V bands. The studied composite significantly reduced reflection. Thus, absorption was dominated in the SE_T in mmWave bands.

4. Conclusions

Microwave absorption property of $Ti_3C_2T_x$ MXene/doped-hexaferrite ($BaCo_{0.3}Ti_{0.3}Fe_{11.4}O_{19}$) composites with various contents (20, 35, and 45 wt%) of doped-hexaferrite was investigated in the frequency range from 30 to 50 GHz for millimeter-wave applications. The

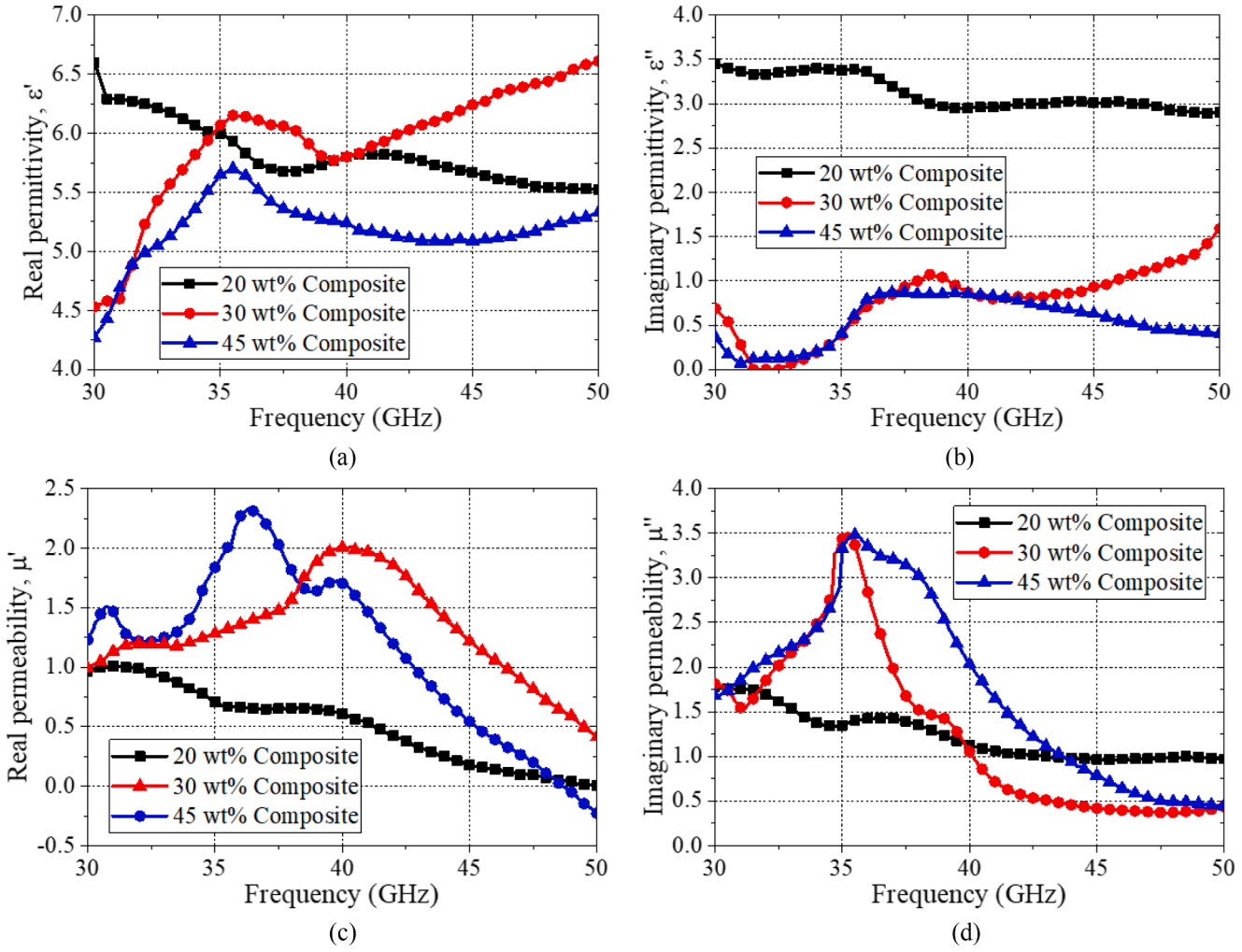

Fig. 5. Dynamic performance of (a) real permittivity, (b) imaginary permittivity, (c) real permeability, and (d) imaginary permeability of MXene/$BaCo_{0.3}Ti_{0.3}Fe_{11.4}O_{19}$ (20, 30, and 45 wt%) composites.

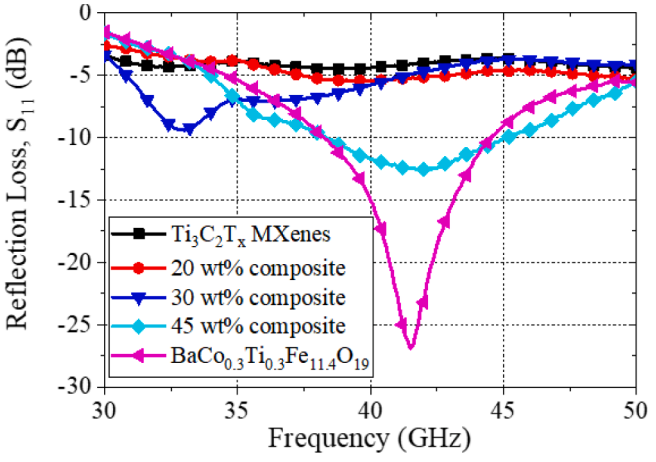

Fig. 6. Reflection loss (S_{11}) of $Ti_3C_2T_x$ MXene, MXene/$BaCo_{0.3}Ti_{0.3}Fe_{11.4}O_{19}$ (20, 30, and 45 wt%) composites, and $BaCo_{0.3}Ti_{0.3}Fe_{11.4}O_{19}$ (CoTi-BaM) with the thickness of 1.5 mm.

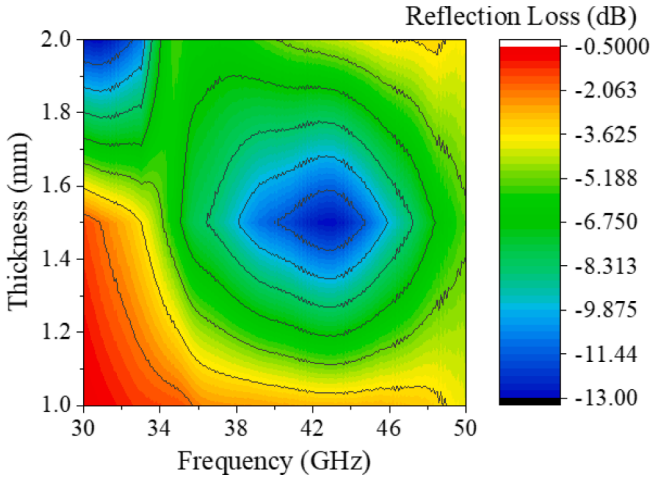

Fig. 7. Reflection loss contour of $Ti_3C_2T_x$ MXene/45 wt% $BaCo_{0.3}Ti_{0.3}Fe_{11.4}O_{19}$ composite with various thicknesses.

1.5 mm thick MXene/doped-hexaferrite (45 wt%) composite shows the highest microwave absorption and shielding effectiveness among the studied composite compositions. An effective absorption bandwidth of 7 GHz (35–45 GHz) was obtained in mmWave bands from the 1.5 mm thick composite. A high-magnetocrystalline anisotropy of hexaferrite contributes to shifting microwave absorption frequency to K_a- and V-bands. Accordingly, the microwave shielding effectiveness was dominated by absorption rather than reflection. Therefore, the reflection

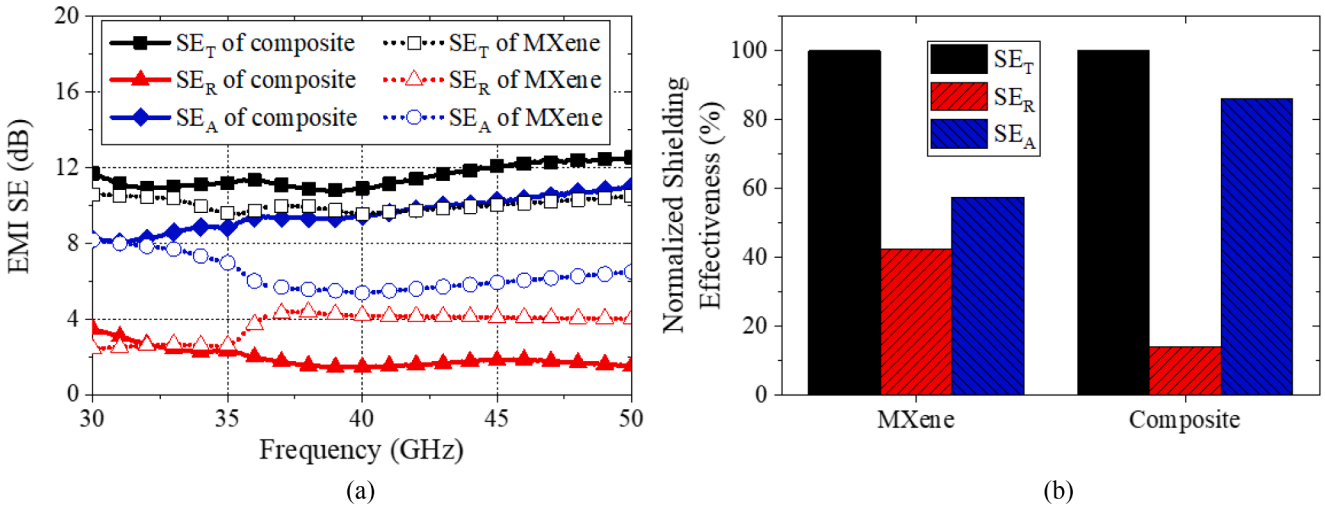

Fig. 8. (a) Shielding effectiveness of 1.5 mm thick $Ti_3C_2T_x$ MXene and MXene/45 wt% $BaCo_{0.3}Ti_{0.3}Fe_{11.4}O_{19}$ composite and (b) normalized shielding effectiveness of 1.5 mm thick MXene and MXene/45 wt% $BaCo_{0.3}Ti_{0.3}Fe_{11.4}O_{19}$ composite at 42 GHz.

Table 1
Comparison of the microwave absorption properties of state-of-the-art and proposed composites.

Single and Composite Materials	Thickness (mm)	RL_{min} (dB)	Frequency at RL_{min} (GHz)	Bandwidth (RL = −10 dB)	Reference
$Sr_{0.85}La_{0.15}(MnZr)_{0.5}Fe_{11}O_{19}$	0.85	−30	34.1	8.72 (29–37.72 GHz)	[23]
$BaCo_{0.5}Ti_{0.5}Fe_{11}O_{19}$	1.16	−20	37.9	9.5 (29–38.5 GHz)	[17]
$Ni_{0.1}Co_{0.9}Fe_2O_4$	1.8	−36.67	31.36	9.5 (26.5–35 GHz)	[24]
$ZnFe_2O_4/SiO_2$/Ppy	1	−36.75	38.38	9.6 (30.4–40 GHz)	[25]
PVDF/Fe_2O_3/Pani-500	3.5	−34	32.5	10 (30–40 GHz)	[26]
$Sr_{0.85}La_{0.15}(NiZr)_{0.5}Fe_{11}O_{19}$	0.96	−21.7	31.5	10.5 (27.5–38 GHz)	[27]
MXene/45 wt% $BaCo_{0.3}Ti_{0.3}Fe_{11.4}O_{19}$	1.5	−12.5	42	7 (38–45 GHz)	This work

issue of MXene is addressed. The experimental results demonstrate that the doped-hexaferrite ($BaCo_{0.3}Ti_{0.3}Fe_{11.4}O_{19}$) composite can apply to EMI shielding in mmWave bands (K_a- and V-bands) and opens up new opportunities for THz EMI materials development.

CRediT authorship contribution statement

Hoyun Won: Conceptualization, Data curation, Formal analysis, Investigation, Methodology, Software, Validation, Visualization, Writing – original draft, Writing – review & editing. **Yang-Ki Hong:** Conceptualization, Formal analysis, Funding acquisition, Investigation, Project administration, Resources, Supervision, Writing – review & editing. **Minyeong Choi:** Writing – review & editing. **Hector Garcia:** Data curation, Software, Validation. **Dongmyung Shin:** Funding acquisition, Project administration, Resources, Supervision. **Young-Sik Yoon:** Funding acquisition, Project administration, Resources, Supervision. **Kwangjoo Lee:** Funding acquisition, Project administration, Resources, Supervision. **Hao Xin:** Supervision. **Chang-Dong Yeo:** Supervision.

Declaration of Competing Interest

The authors declare the following financial interests/personal relationships which may be considered as potential competing interests: Yang-Ki Hong reports financial support was provided by National Science Foundation.

Acknowledgements

This work was supported in part by the National Science Foundation - IUCRC under Grant number 1650564.

References

[1] D. Chung, Electromagnetic interference shielding effectiveness of carbon materials, Carbon 39 (2) (2001) 279–285.
[2] Y. Lei, Z. Yao, S. Li, J. Zhou, A. Haidry, P. Liu, Broadband high-performance electromagnetic wave absorption of Co-doped NiZn ferrite/polyaniline on MXene, Ceram. Int. 46 (8) (2020) 10006–10015.
[3] J. He, D. Shan, S. Yan, H. Luo, C. Cao, Y. Peng, Magnetic FeCo nanoparticles-decorated Ti_3C_2 MXene with enhanced microwave absorption performance, J. Magn. Magn. Mater. 492 (2019) 165639.
[4] D. Shan, J. He, L. Deng, S. Yan, H. Luo, S. Huang, Y. Xu, The underlying mechanisms of enhanced microwave absorption performance for the $NiFe_2O_4$-decorated $Ti_3C_2T_x$ MXene, Results Phys. 15 (2019) 102750.
[5] J. He, S. Liu, L. Deng, D. Shan, C. Cao, H. Luo, S. Yan, Tunable electromagnetic and enhanced microwave absorption properties in $CoFe_2O_4$ decorated Ti_3C_2 MXene composite, App. Surface Sci. 504 (2020) 144210.
[6] M. Han, C.E. Shuck, R. Rakhmanov, D. Parchment, B. Anasori, C.M. Koo, G. Friedman, Y. Gogotsi, Beyond $Ti_3C_2T_x$: MXene for electromagnetic interference shielding, ACS Nano. 14 (4) (2020) 5008–5016.
[7] M. Naguib, V. Mochalin, M. Barsoum, Y. Gogotsi, 25th Anniversary Article: MXene: A new family of two-dimensional materials, Adv. Mater. 26 (7) (2014) 992–1005.
[8] P. Pham, W. Zhang, N. Quach, J. Li, W. Zhou, D. Scarmardo, E. Brown, P. Burke, Broadband impedance match to two-dimensional materials in the terahertz domain, Nat. Commun. 8 (2017) 2233.
[9] F. Shahzad, M. Alhabeb, C. Hatter, B. Anasori, S. Hong, C. Koo, Y. Gogotsi, Electromagnetic interference shielding with 2D transition metal carbides (MXene), Science 353 (6304) (2016) 1137–1140.
[10] G. Park, D. Ho, B. Lyu, S. Jeon, D. Ryu, D. Kim, N. Lee, S. Kim, Y. Song, S. Jo, J. Cho, Comb-type polymer-hybridized MXene nanosheets dispersible in arbitrary polar, nonpolar, and ionic solvents, Sci. Adv. 8 (2022) 1–8.
[11] L. Liang, G. Han, Y. Li, B. Zhao, B. Zhou, Y. Feng, J. Ma, Y. Wang, R. Zhang, C. Liu, Promising $Ti_3C_2T_x$ MXene/Ni chain hybrid with excellent electromagnetic wave absorption and shielding capacity, ACS Appl. Mater. Interfaces 11 (28) (2019) 25399–25409.
[12] F. Pan, L. Yu, Z. Xiang, Z. Liu, B. Deng, E. Cui, Z. Shi, X. Li, W. Lu, Improved synergistic effect for achieving ultrathin microwave absorber of 1D Co nanochains/2D carbide MXene nanocomposite, Carbon 172 (2021) 506–515.
[13] B. Deng, L. Wang, Z. Xiang, Z. Liu, F. Pan, W. Lu, Rational construction of MXene/Ferrite@C hybrids with improved impedance matching for high-performance electromagnetic absorption applications, Mater. Lett. 284 (2021) 129029.

[14] Y. Li, X. Zhou, J. Wang, Q. Deng, M. Li, S. Du, Y. Han, J. Lee, Q. Huang, Facile preparation of in situ coated Ti3C2Tx/$Ni_{0.5}Zn_{0.5}Fe_2O_4$ composites and their electromagnetic performance, RSC Adv. 7 (40) (2017) 24698–24708.
[15] Y. Peng, L. Deng, P. Zhang, X. Gao, S. Huang, S. Fang, T. Qin, C. Li, Tunable and broadband high-performance microwave absorption of $ZnFe_2O_4$ nanoparticles decorated $Ti_3C_2T_x$ MXene composites, J. Magn. Magn. Mater. 541 (2022) 168544.
[16] J. Kim, Y. Kang, Synthesis, characterization, and electromagnetic wave absorbing properties of M_1[1] -M_2^{3+} substituted M-type Sr-Hexaferrites, Appl. Sci. 11 (18) (2021) 8669.
[17] C. Dong, X. Wang, P. Zhou, T. Liu, J. Xie, L. Deng, Microwave magnetic and absorption properties of M-type ferrite $BaCo_xTi_xFe_{12-2x}O_{19}$ in the Ka band, J. Magn. Magn. Mater. 354 (2014) 340–344.
[18] L. Wang, R. Zhou, H. Xin, Microwave (8–50 GHz) characterization of multiwalled carbon nanotube papers using rectangular waveguides, IEEE Trans. Microw. Theory Techn. 56 (2) (2008) 499–506.
[19] S. Guo, H. Guan, Y. Li, Y. Bao, D. Lei, T. Zhao, B. Zhong, Z. Li, Dual-loss $Ti_3C_2T_x$ MXene/$Ni_{0.6}Zn_{0.4}Fe_2O_4$ heterogeneous nanocomposites for highly efficient electromagnetic wave absorption, J. Alloy Comp. 887 (2021) 161298.
[20] X. Zhang, H. Wang, R. Hu, C. Huang, W. Zhong, L. Pan, Y. Feng, T. Qiu, C. Zhang, J. Yang, Novel solvothermal preparation and enhanced microwave absorption properties of $Ti_3C_2T_X$ MXene modified by in situ coated Fe_3O_4 nanoparticles, Appl. Surf. Sci. 484 (2019) 383–391.
[21] C. Caloz, T. Itoh, Electromagnetic Metamaterials: Transmission Line Theory and Microwave Applications, Wiley-IEEE Press, New York, NY, USA, 2005.
[22] G. Weng, J. Li, M. Alhabeb, C. Karpovich, H. Wang, J. Lipton, K. Maleski, J. Kong, E. Shaulsky, M. Elimelech, Y. Gogotsi, A. Taylor, Layer-by-layer assembly of cross-functional semi-transparent MXene-Carbon nanotubes nanotubes composite films for next-generation electromagnetic interference shielding, Adv. Func. Mater. 28 (2018) 18033160.
[23] P. Kaur, S. Bahel, S. Narang, Broadband microwave absorption of $Sr_{0.85}La_{0.15}(MnZr)_xFe_{12-2x}O_{19}$ hexagonal ferrite in 18–40 GHz frequency range, J. Magn. Magn. Mater. 460 (2018) 489–494.
[24] K. Pubby, S.B. Narang, Ka band absorption properties of substituted nickel spinel ferrites: comparison of open-circuit approach and short-circuit approach, Ceram. Int. 45 (2019) 23673–23680.
[25] Y. Ge, C. Li, G.I.N. Waterhouse, Z. Zhang, L. Yu, $ZnFe_2O_4$@SiO_2@Polypyrrole nanocomposites with efficient electromagnetic wave absorption properties in the K and Ka band regions, Ceram. Int. 47 (2) (2021) 1728–1739.
[26] F. Liu, C. Li, G. Waterhouse, X. Jiang, Z. Zhang, L. Yu, Lightweight PVDF/γ-Fe2O3/PANI foam for efficient broadband microwave absorption in the K and Ka bands, J. Alloys Compd. 876 (2021) 159983–159992.
[27] P. Kaur, S.B. Narang, S. Bahel, Enhanced microwave absorption properties of Ni-Zr doped La-Sr hexagonal ferrites in 18–40 GHz frequency range, Mater. Sci. Eng. B. 268 (2021).